Deep Learning Based Topography Aware Gas Source Localization with Mobile Robot

Changhao Tian[1,2,5,*], Annan Wang[3,*], Han Fan[4], Thomas Wiedemann[5,6], Yifei Luo[2], Le Yang[2,7,‡], Weisi Lin[3,‡], Achim J. Lilienthal[4,5,‡], Xiaodong Chen[1,8,‡]

***Abstract*—Gas source localization in complex environments is critical for applications such as environmental monitoring, industrial safety, and disaster response. Traditional methods often struggle with the challenges posed by a lack of environmental topography integration, especially when interactions between wind and obstacles distort gas dispersion patterns. In this paper, we propose a deep learning-based approach, which leverages spatial context and environmental mapping to enhance gas source localization. By integrating Simultaneous Localization and Mapping (SLAM) with a U-Net-based model, our method predicts the likelihood of gas source locations by analyzing gas sensor data, wind flow, and topography of the environment represented by a 2D occupancy map. We demonstrate the efficacy of our approach using a wheeled robot equipped with a photoionization detector, a LIDAR, and an anemometer, in various scenarios with dynamic wind fields and multiple obstacles. The results show that our approach can robustly locate gas sources, even in challenging environments with fluctuating wind directions, outperforming conventional methods by utilizing topography contextual information. This study underscores the importance of topographical context in gas source localization and offers a flexible and robust solution for real-world applications.**

***Index Terms*—Gas Source Localization, Robot Olfaction, Machine Olfaction, Cognitive Robotics, Deep Learning, Simultaneous Localization and Mapping (SLAM)**

[1]Innovative Center for Flexible Devices (iFLEX), Max Planck-NTU Joint Laboratory for Artificial Senses, School of Materials Science, Nanyang Technological University, Singapore

[2]Institute of Materials Research and Engineering, Agency for Science, Technology and Research, Singapore

[3]College of Computing and Data Science, Nanyang Technological University, Singapore

[4]Robot Navigation and Perception Lab, AASS Research Centre, Örebro University, Sweden

[5]Chair: Perception for Intelligent Systems, Munich Institute of Robotics and Machine Intelligence (MIRMI), Technical University of Munich, Germany

[6]Institute of Communications and Navigation, German Aerospace Center (DLR), Germany

[7]Department of Materials Science and Engineering, National University of Singapore, Singapore

[8]Institute for Digital Molecular Analytics and Science (IDMxS), Nanyang Technological University, Singapore

*Changhao Tian and Annan Wang contributed equally to this work.

‡Corresponding authors: Le Yang (yang_le@imre.a-star.edu.sg), Weisi Lin (wslin@ntu.edu.sg), Achim J. Lilienthal (achim.j.lilienthal@tum.de), and Xiaodong Chen (chenxd@ntu.edu.sg).

The authors acknowledge the financial support from the Singapore Agency for Science, Technology and Research (A*STAR) under its MTC Programmatic Funding Scheme (project no. M23L8b0049) Scent Digitalization & Computation (SDC) Programme, and the funding from the academic program Sustainable Underground Mining (SUM) project, jointly financed by LKAB and the Swedish Energy Agency.

I. Introduction

Among different scenarios, ranging from environmental monitoring [1], industrial safety [2], and disaster rescue [3], dispersed gas is always an important but invisible environmental factor. Detecting and locating potential gas sources is crucial for ensuring environmental compliance, preventing industrial accidents, and supporting rescue operations. Therefore, using mobile robots committing gas source localization in hazardous or hard-to-reach environments becomes appealing.

A robot for gas source localization typically uses a gas sensor to detect the gas transmitted from the source and an anemometer to estimate the direction of the source. However, real-world scenarios can be challenging as gas source localization is often a non-observable estimation problem [4]. This is because observed gas concentrations and airflow vectors do not directly correlate with the source location due to complex wind-obstacle interactions. Early in gas dispersion, a continuous concentration gradient has not yet formed and turbulence creates plumes with fluctuating concentrations [5], [6]. This means observed gas concentrations only indicate the presence of gas, not the distance to the source. Additionally, obstacles distort wind streamlines, making it difficult to infer source direction solely from anemometer data. As a result, gas source localization in complex environments with obstacles is challenging due to the limitations of sensory information.

To address this obstacle-induced challenge, we consider leveraging spatial context such as the environmental topography and observed wind flow to learn the complex, non-analytical relationship between gas encounters and the actual gas source location. The contextual information in environmental topology can be perceived by Simultaneous Localization and Mapping (SLAM), which allows robots to create or update maps of unknown environments while tracking their location [7]. For gas source localization, SLAM can contribute with accurate locations where gas is detected and corresponding surrounding topography [8]. Assuming that obstacle layout affects the gas dispersal process and therefore is crucial for predicting gas source locations, integrating SLAM could greatly enhance the localization process.

In this work, we propose a deep learning-based approach for gas source localization in complex environments. The goal of our work is to train a model that can predict the potential gas source location during the SLAM process when the robot encounters the plume, leveraging data from a LIDAR, an anemometer, and a gas sensor. As depicted in Fig. 1, the envi-

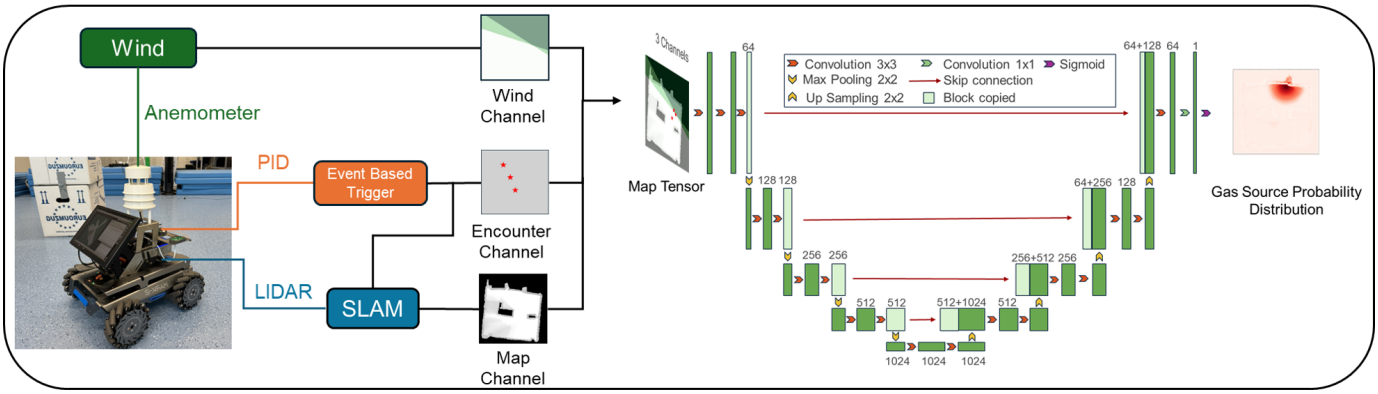

Fig. 1. Overview of the gas source localization system. Our topography-aware approach leverages gas plume encounter data and corresponding contextual information (environmental topography and wind conditions) and can use newly detected gas encounters to predict the gas source location in real time.

ronment map, gas encounter locations and wind observations will be combined into a 3-channel tensor and put into a U-Net, which can capture the topography context related to gas dispersion. When the robot is deployed to an unknown environment, the model can predict the potential locations of gas sources despite a different topography. To implement and demonstrate our approach, we built a wheeled mobile robot equipped with a photoionization detector (PID), an anemometer, and a LIDAR and conducted real-world experiments. We have shown that our method can locate the gas source effectively in an environment with multiple obstacles and complex gas plume distribution. Even under a changing wind field, our method can remain robust.

The main contribution of this paper is the exploitation of the topography context for gas source localization, which allows our approach to address the challenges posed by the intractable interaction between obstacles and wind fields. This contribution can extend the flexibility and applicability of gas source localization robots in realistic scenarios with the potential of predicting gas source locations from a distance without continuous active tracing.

II. Related Work

The localization of gas sources in complex environments has been a longstanding challenge in the field of mobile robot olfaction. Conventional approaches are unable to handle complex interaction patterns between dispersed gas and environmental topography. Recent advances in deep learning offer a promising solution by approximating these complex patterns and their relationship to the source location, motivating the development of novel learning-based localization approaches.

A. Properties of Gas Plume

In gas source localization, a gas source is typically modelled as a point source with dispersion influenced by turbulent fluid flows rather than diffusion. The gas plume can be described as follows: 1) It originates from a point source and follows the wind gradient. 2) Gas concentrations fluctuate due to turbulence, with the highest average concentration along the plume's centerline. 3) Unlike natural diffusion, the plume exhibits patchy concentration levels rather than a smooth gradient. As a result, the presence of a plume is a more reliable indicator of the gas source than a concentration gradient. Some studies model gas plumes analytically [9], [10] or statistically [11], [12], while others focus on plume tracking strategies [6]. Early plume tracking methods aim to keep robots in contact with the plume, such as adjusting speed or direction when losing contact [13], [14]. These methods fall under reactive source localization, discussed in Section II-B.

B. Reactive Gas Source Localization

Reactive methods in robotics involve responding to real-time sensor data with predefined actions, without relying on historical data or dynamic analysis. These approaches are simple, resource-efficient, and adaptable to various platforms [15]. A typical reactive method for gas source localization is chemotaxis [16], where a robot moves toward higher gas concentrations. However, this assumes a continuous concentration gradient, which may not exist in turbulent gas dispersal. An improved version, chemotaxis-anemotaxis [17], uses both gas concentration and wind direction. Bio-inspired strategies like upwind surging and crosswind zigzagging guide the robot [6], [18]. Despite their simplicity, reactive methods often limit flexibility and efficiency, particularly in challenging environments like disaster sites with obstacles and rough terrain. In multi-purpose missions, robots may need to follow specific paths, making it impractical to continuously trace a gas source. In such cases, predicting gas source locations from a distance during exploration becomes more feasible.

C. Statistical Gas Source Localization

Statistical methods address the limitations of reactive approaches by using probabilistic models to estimate the gas source location [4], [19]. These methods integrate sensor data with environmental models and prior knowledge, employing techniques like Bayesian filtering [20], Kalman filtering [21], and particle filtering [19], [22] to update beliefs as new measurements are observed. One state-of-the-art approach, Infotaxis, optimizes source search by maximizing information gain at each step [23]–[25].

In general, statistical methods account for the often meandering and fluctuating gas dispersion and offer the advantage of providing estimates along with uncertainty measures. However, their applicability also has limitations [23], [26]. The major issue is the strong dependence on an accurate gas dispersion model. For example, a common assumption is a uniform wind field, where all points in the field are considered to have the same wind vector. However, this assumption probably will not hold in complex, varying and uncontrolled environmental conditions.

D. Learning-based Gas Source Localization

Deep learning has become a prominent tool in robotic applications due to its ability to make effective decisions with limited data [27]. Methods such as deep Q networks (DQN) [28], [29] and long short-term memory networks (LSTMs) [30] demonstrated promising results in gas source localization problems. Inspired by the success of image segmentation models like U-Net [31], Mask R-CNN [32], and DeepLab [33] in extracting spatial relationships from images, we propose leveraging contextual information embedded in metric maps to enhance gas source localization predictions based on in-situ and sparse observations.

III. Methodology

We develop a gas source localization approach based on an environmental context-aware U-net. The training of the approach is twofold. In the first phase (Section III-A), a series of samples are acquired. Once the robot encounters a gas plume in the environment, the gas sensor signal will be processed by an event-based filter to trigger data collection. Corresponding environmental context, i.e., the current metric map and encounter locations perceived by SLAM, and wind direction from an anemometer will be recorded. In the second phase (Section III-B), we train the U-net to capture the relationship between the environmental context and the source location. The resulting context-aware U-net is the predictive model that can estimate a probabilistic representation of the gas source location.

A. Event-based Human-in-the-loop Data Collection

The model training starts with collecting representative data that encoded the tempo-spatial pattern of the plume(s) released by the gas source. We assume that this pattern can be indirectly reflected by the gas sensor responses, the corresponding position and the observed wind flow when the robot encounters a plume. The determination of plume encounters is a twofold process. First, potential encounters are detected by an event-based filter. Then, the detected encounters are validated by a human operator, to avoid repeated recording near the same location. The implementation of the event-based filter is given by Eq. 1 and Eq. 2, proposed by Li et al. [34], as follows:

$$C_{\text{filtered}} = \begin{cases} 1, & \text{if } c_t > k\bar{c}_{t-1} \\ 0, & \text{if } c_t \leq k\bar{c}_{t-1} \end{cases} \tag{1}$$

$$\bar{c}_t = \gamma\bar{c}_{t-1} + (1-\gamma)c_t \tag{2}$$

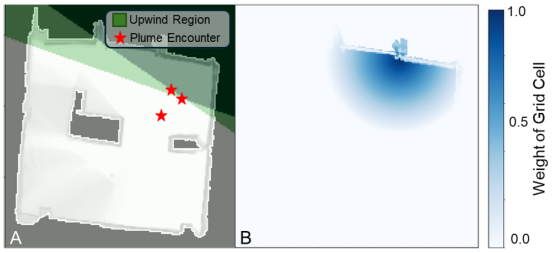

Fig. 2. An example of the map tensor and grid cells' weight in loss calculation. **(A)**: A 3-channel map tensor includes a metric map, gas encounter locations and the wind direction belief. A deeper green colour means a higher belief in the upwind region. **(B)**: An exemplary visualization of the weights of the grids in the loss function. Inside a dynamic detecting range (blue area), grids near the edge will be assigned smaller weights.

where c_t is the sensor response at time t, k is a predefined noise threshold, and γ is a trade-off parameter that controls the filter sensitivity. This filter will covert continuous sensor readings to binary numbers that indicate plume encounter events. With adaptive threshold $\bar{c}_t$, the filter can detect plumes effectively, without being affected by the accumulative gas in the environment. In our experiment, the sampling frequency of the gas sensor was set at 1Hz, γ was set as 0.2, and k was set as 1.04. These hyperparameters were determined during preliminary experiments to avoid false positive triggers. When the filter returns a value of 1, the encounter location is recorded only after confirmation by the operator. This step is taken to avoid excessively repeated triggers at the same location when the robot is close to the gas source.

The training data requires several trials. A trial is referred to as a mapping process from an initially empty map. During one trial, when a plume encounter is confirmed. The current occupancy map, the corresponding location of the robot in the map, and the data from the anemometer will be saved. At the end of a trial, the robot is guided to the gas source location, and the location of the robot on the map is recorded to represent the true position of the gas source.

B. Training Setup

Data Prepossessing: For each recorded gas encounter, a sample is stored as a map tensor with three channels: the map, encounter, and wind. The map channel records the metric map (occupancy grid map) at the encounter moment. To standardize inputs, maps are padded with -1 to a uniform shape. The robot's position at the gas encounter is represented using the baselink-to-map transformation, indicating the encounter pose. The encounter channel, with the same size as the occupancy grid map, marks the encounter coordinates with a value of 1, and all other grids as 0. For each map, all encounters up to that point are marked. During each trial, a sequence of samples is generated in the order of their encounters.

The information in the wind channel plays an important role in gas source localization. Assuming that gas often disperses from the upwind direction to the downwind direction, when a single gas source is presented, the probability of the gas source being located in the downwind region related to a plume encounter point is much lower than in the upwind region.

In our implementation of the wind channel, the anemometer data is a vector $\vec{V}_{\text{wind}}$ pointing to the upwind direction. Each encounter's wind field matrices will be an array of the same shape as the map. Eq. 3 defines the value W_i for each grid cell based on its orientation relative to the wind direction. A grid cell is considered upwind if the dot product of its vector $\vec{V}_i$ with the wind vector, $\vec{V}_{\text{wind}}$, is greater than or equal to 0, and downwind if the dot product is less than 0. The wind channel serves as a cumulative representation of all encountered wind field matrices over time. It provides a comprehensive overview of each grid's state in terms of the wind condition.

$$W_i = \begin{cases} 1, & \text{if } \vec{V}_{\text{wind}} \cdot \vec{V}_i \geq 0 \\ -1, & \text{if } \vec{V}_{\text{wind}} \cdot \vec{V}_i < 0 \\ 0, & \text{if } \vec{V}_{\text{wind}} = 0 \end{cases} \tag{3}$$

To enhance model robustness, all samples are rotated clockwise by $\frac{\pi}{2}, \pi, \frac{3\pi}{2}$ radians for data augmentation. Fig. 2(A) is a visualization of the map tensor sample corresponding to the 3rd encounter event in a trial.

Source Posterior Map and Loss Function: The model's expected output is a source posterior map, a probabilistic representation of the gas source location. Each grid cell in this map holds a value indicating the probability of containing a gas source, accounting for uncertainty in real-world localization. Since predicting the source location can vary in difficulty depending on encounters and SLAM map completeness, we introduce a dynamic detection range, D_N, given by Eq. 4, to reduce training instability caused by difficulty,

$$D_N = a \cdot e^{-k \cdot (N-1)} + c \tag{4}$$

where N represents the number of plume encounters in the current map. The parameter a is set to 3, and c is set to 1, meaning that the dynamic detecting range D_N starts at 4 meters after the first encounter and gradually converges to a 1 meter range as the number of encounters increases. k, representing the convergence rate, is set to 0.3.

The training loss is defined based on Binary Cross-Entropy (BCE), Eq. 5, a commonly used function in binary classification tasks. The goal is for the model to predict the region inside D_N, rather than exact source coordinates.

$$\text{BCE}(y_i, \hat{y}_i) = y_i \log(\hat{y}_i) + (1 - y_i) \log(1 - \hat{y}_i) \tag{5}$$

However, manually defined regions are not absolutely accurate, and the model may struggle to align precisely at the edges, leading to instability during training. To ensure smoother training, it is necessary to reduce the weights at the edges of the predicted region.

Each grid is assigned a weight as Eq. 6:

$$y_{N,i} = \begin{cases} 0, & \text{if } d_i > D_N \text{ or } m_i = -1 \\ \frac{(D_N - d_i)}{D_N} \cdot \frac{(100 - m_i)}{100}, & \text{if } d_i \leq D_N \end{cases} \tag{6}$$

in which d_i is the distance between grid i and the gas source location, m_i is the value of grid i. All grids outside D_N range of the gas source are labelled as 0, while grids inside D_N range

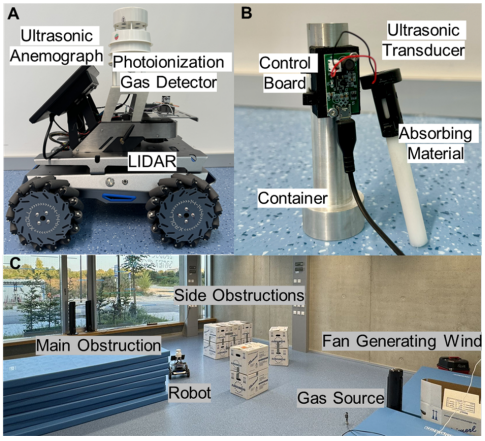

Fig. 3. Experimental setup. **(A)**: The wheeled mobile robot is equipped with a PID, an anemometer, and a LIDAR. **(B)**: The artificial ethanol source. **(C)**: The experiment scenario.

are labelled as $\frac{(D_N - d_i)}{D_N} \cdot \frac{(100 - m_i)}{100}$, considering both distance to gas source and occupancy probability of the map, as shown in Fig. 2(B).

The training loss is defined as :

$$\text{Loss} = -\frac{1}{n} \sum_{i=1}^{n} \text{loss}(y_i, \hat{y}_i) \tag{7}$$

$$\text{loss}(y_i, \hat{y}_i) = \begin{cases} \text{BCE}(y_i, 0), & \text{if } \hat{y}_i = 0 \\ \hat{y}_i^{\frac{1}{5}} \cdot \text{BCE}(y_i, 1) \cdot \text{W}_{\text{pos}}, & \text{if } \hat{y}_i > 0 \end{cases} \tag{8}$$

The loss function, Eq. 7, 8 first computes the binary classification loss for the region in the range D_N, and then adjusts it using the decreased weight $\hat{y}_i^{\frac{1}{5}}$ and a positive weighting factor. The W_{pos} is set as 5.0, assigning a higher weight to the positive sample in case of imbalanced sample distribution.

Training of Gas Localization Predictive Model: We selected U-Net as our backbone model due to its effectiveness in image segmentation, characterized by a U-shaped architecture that captures spatial context [31]. The dataset was split into training and validation sets with a 4:1 ratio, ensuring robust evaluation. To prevent data leakage, samples from the same trial were kept within the same set. Our U-Net model features a symmetric encoder-decoder structure with 23 convolutional layers. The encoder includes four downsampling steps, each with two 3x3 convolutions, batch normalization, and ReLU activation. The feature map size is halved with 2x2 max-pooling at each step, starting with 64 channels and doubling at each layer. The bottleneck has 1024 channels. The decoder mirrors the encoder, using transposed convolutions for upsampling and concatenating with corresponding encoder features. The final 1x1 convolution layer outputs the desired number of classes, with a sigmoid function converting the output into a probability distribution. The U-net converged stably after 100 epochs, with a batch size of 8 and an initial learning rate of $1e-5$. Learning rate halving and L2 regularization with a weight decay of 0.01 were also applied to avoid overfitting.

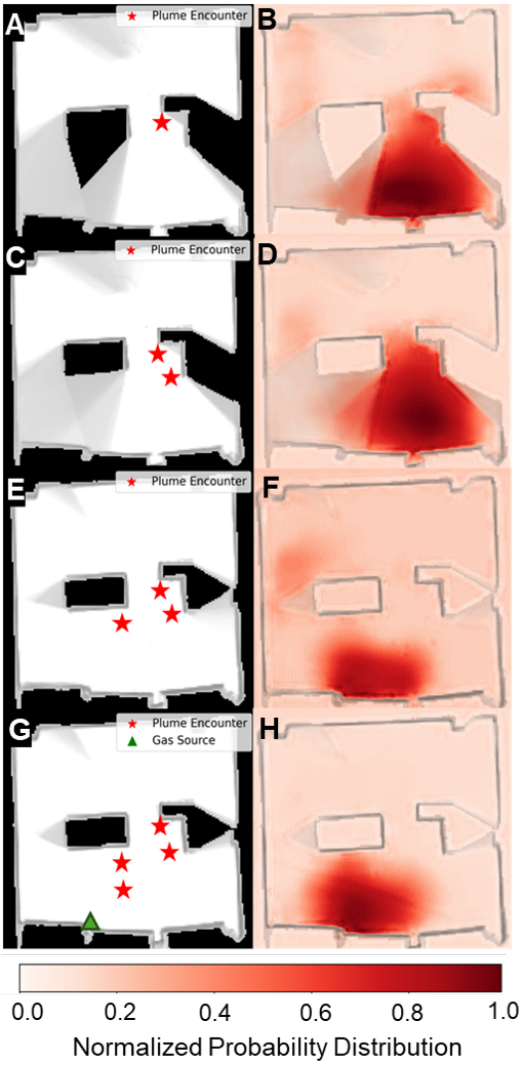

Fig. 4. Model performance in one trial with increasing encounters and map completeness. The model's output demonstrates improved prediction accuracy and continuity as more gas encounters are acquired (Fig. 4(A), (C), (E) and (G)) and the coverage of the source posterior map increases (Fig. 4(B), (D), (F) and (H)). When 4 encounters were acquired (see (Fig. 4(G)), the grids assigned with the highest posteriors in Fig. 4(H) align closely with the actual source.

IV. Experimental Setup

A. Robotic platform and sensor payloads

The robotic platform is built on a Mecanum wheel chassis, shown by Fig. 3(A). It is equipped with a CZ0001 ultrasonic anemometer, an LDS-250D laser LIDAR, and a PID-AH2 gas sensor. The CZ0001 ultrasonic anemometer allows to collect wind in the speed range of 0 to 40 m/s with an angular accuracy of ±2°, a speed accuracy of ±2% and a speed threshold of 0.05 m/s. The LDS-25D can generate point clouds of up to 14000 points per second with a 30 m range with an accuracy of ±0.01m at 14k Hz. The PID-AH2 is a highly sensitive photoionization detector (PID). A PID uses an ultraviolet (UV) lamp to ionize a detectable compound, including most Volatile Organic Compounds (VOCs) [35]. In our experiment, the PID-AH2 has a detection range from sub 1 parts per billion (ppb) to 50 parts per million (ppm).

All the sensor payloads are controlled by an NVIDIA Jetson Nano embedded processor. The robot's movement can be controlled via a remote controller. The SLAM functionality was implemented using the off-the-shelf Cartographer ROS package [7].

B. Target gas source and area

The target gas is generated by an ultrasonic ethanol vaporizer (see Fig. 3(B)). Ethanol liquid in the container contacts an ultrasonic transducer through an absorbent material, producing ethanol vapour at room temperature. Near the ground surface, the gas can remain at a relatively constant altitude while being dispersed by wind currents without significant vertical floating via temperature gradient.

The experimental setup, depicted in Fig. 3(C), consisted of an empty room measuring 10 meters by 10 meters. To facilitate gas dispersion, an artificial wind field was generated using three fans. A large central obstacle was introduced to alter the overall wind flow pattern, while smaller side obstacles were placed to influence the finer details of the resulting gas plume shape. All obstacles were higher than the fans to prevent airflow from bypassing them. The experiment was conducted under various conditions, including different fan configurations, gas source locations, obstacle arrangements, and initial robot positions

V. Results and Discussion

This section presents the qualitative and quantitative evaluation results of our approach. We conducted 60 trials to gather sufficient training data, and the trained model was then deployed on the robot for gas source localization in real-world trials with previously unseen obstacle layouts and sources. In 8 testing trials with stable wind and 8 testing trials with changing wind, the model successfully inferred gas source locations based on fused map data (see Section V-A). To assess generalization, we tested the model in environments with changing wind fields. As detailed in Section V-B, the results validated the model's robustness, demonstrating its ability to perform fuzzy inference in dynamic environments. The evaluation showcases that spatial context-based inference is an effective approach for gas source localization.

A. Inference with Spatial Context

In testing, our approach performed accurate gas source localization within 4 plume encounters, as the example shown by Fig. 4. This is based on two key factors: a more complete map and an increased number of plume encounter locations. When encountering a plume, the model infers the probability distribution of the gas source within the explored area. Once the environment around the gas source is scanned, from Fig. 4A to Fig. 4C, the probability distribution becomes more continuous and is associated with a higher confidence level. As the number of encounters increases, the predicted probability distribution gradually converges, whose high-valued grids begin to overlap on the area surrounding the actual gas source.

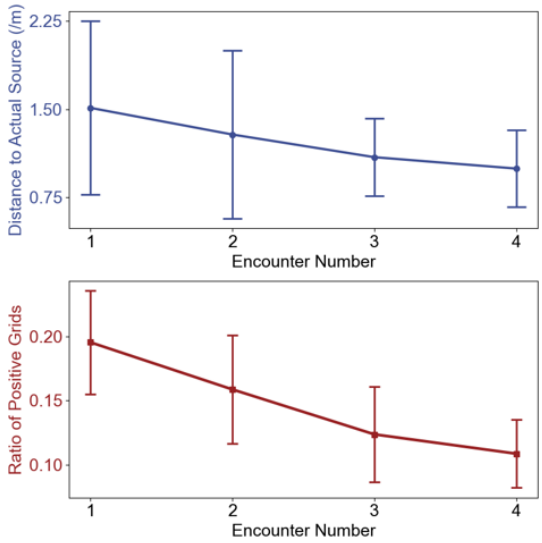

Fig. 5. Quantitative evaluation of the output of the model in testing trials: with increasing number of encounters, both the distance to the actual gas source and the ratio of positive grids decreases, indicating both model's belief and accuracy increase with a more complete spatial context.

With a sufficient number of plume encounters, the model gathers enough spatial context to accurately infer the likely gas source area and, therefore predict potential gas source location.

To evaluate the model's performance, we analyzed how its output changes with the number of encounters in the testing set. Two indices were defined for this analysis: the ratio of positive grids and the distance from the centroid of the probability distribution to the actual gas source. The ratio of positive grids measures the proportion of grid cells with probability values greater than 0.5, indicating the model's confidence. The centroid of the probability distribution is used to compute the distance to the actual gas source, which quantifies the model's accuracy. This index is calculated by weighting each grid cell by its predicted probability. As shown by Fig. 5, the result shows that with the first encounter, both the mean value and spread of distance to the actual gas source are large, reflecting a high uncertainty and lower accuracy. As the number of encounters increases, both the mean distance and the spread significantly decrease. Additionally, the ratio of positive grids decreases significantly with the number of encounters, indicating that the predicted gas source area is converging to a smaller area. Given the fact that more acquired encounters often bring more corresponding spatial and wind condition contexts, this result also implies that contextual information is crucial for improving the model prediction.

B. Handling Dynamic Wind Fields

To further evaluate the robustness of our method, we conducted tests in dynamic wind fields, where oscillating fans created a swinging wind pattern. As shown in Fig. 6, the robot accurately localized the gas source despite the changing wind conditions in two testing trials. Note that the training data were all generated with non-dynamic wind conditions, and the anemometer can only provide in-situ local airflow measurements. Nevertheless, our approach is still able to

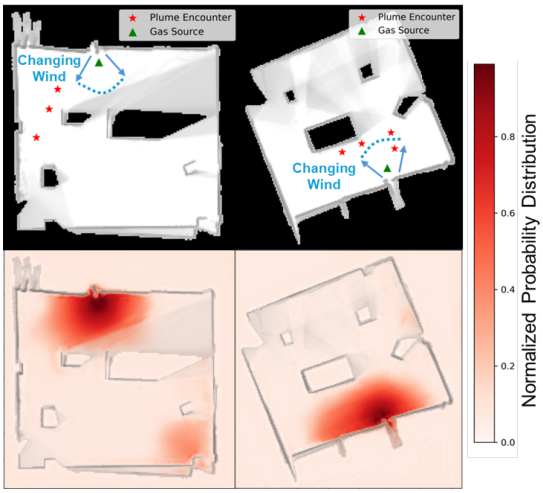

Fig. 6. Results of two test trials posed with changing wind field (shown by blue arrows). In dynamic environments that were never included in the training, our approach remains robust in terms of prediction accuracy.

perform prediction from encounter events and corresponding contextual information. The success achieved in dynamic wind conditions further emphasizes the importance of spatial context in gas source localization. Our approach is promising with its robustness and broader applicability in complex, uncontrolled real-world environments.

VI. Conclusion and Outlook

In this work, we presented a topography-aware gas source localization approach based on U-Net. Our approach leverages the environmental context to learn the intractable relationship between gas encounter events and the source location. We demonstrated that our method has a robust performance under complex and dynamic conditions in real-world experiments. To the best of our knowledge, few related works can be used as a directly comparable benchmark. Extracting hotspots from a statistical gas distribution map offers a relevant reference point for our work [3], [8]. However, using these statistical gas distribution mapping-based methods often requires traversing the environment. We plan to compare and integrate our approach with these methods to explore potential synergies.

Currently, the 2D environmental representation relies on the assumption of wind flow around, rather than over obstacles. To achieve more comprehensive gas spatial perception, future work could involve using 3D LIDAR or stereo cameras to obtain a 3D occupancy grid map. Besides, future work will need to address the challenges of multiple or moving gas sources in the environment. Currently, the success of our approach is based on the assumption of a single gas source. When there are multiple potential gas sources of interest, the sufficiency of inferring the gas source location based solely on encounter positions and their contextual information may be challenged. Overall, our findings suggest that environmental context-based inference is a promising approach to improving gas source localization of mobile robots.

REFERENCES

[1] T. Lewis and K. Bhaganagar, "A comprehensive review of plume source detection using unmanned vehicles for environmental sensing," *Science of the Total Environment*, vol. 762, p. 144029, 2021.

[2] R. K. Kodali, R. Greeshma, K. P. Nimmanapalli, and Y. K. Y. Borra, "Iot based industrial plant safety gas leakage detection system," in *2018 4th international conference on computing communication and automation (ICCCA)*. IEEE, 2018, pp. 1–5.

[3] H. Fan, V. Hernandez Bennetts, E. Schaffernicht, and A. J. Lilienthal, "Towards gas discrimination and mapping in emergency response scenarios using a mobile robot with an electronic nose," *Sensors*, vol. 19, no. 3, p. 685, 2019.

[4] P. Ojeda, J. Monroy, and J. Gonzalez-Jimenez, "Robotic gas source localization with probabilistic mapping and online dispersion simulation," *IEEE Transactions on Robotics*, 2024.

[5] N. Arnold, J. Gruber, and J. Heitz, "Spherical expansion of the vapor plume into ambient gas: an analytical model," *Applied Physics A*, vol. 69, pp. S87–S93, 1999.

[6] G. Kowadlo and R. A. Russell, "Robot odor localization: a taxonomy and survey," *The International Journal of Robotics Research*, vol. 27, no. 8, pp. 869–894, 2008.

[7] W. Hess, D. Kohler, H. Rapp, and D. Andor, "Real-time loop closure in 2d lidar slam," in *2016 IEEE international conference on robotics and automation (ICRA)*. IEEE, 2016, pp. 1271–1278.

[8] K. Kamarudin, A. Y. Md Shakaff, V. H. Bennetts, S. M. Mamduh, A. Zakaria, R. Visvanathan, A. S. Ali Yeon, and L. M. Kamarudin, "Integrating slam and gas distribution mapping (slam-gdm) for real-time gas source localization," *Advanced Robotics*, vol. 32, no. 17, pp. 903–917, 2018.

[9] H. Ishida, T. Nakamoto, and T. Moriizumi, "Remote sensing and localization of gas/odor source and distribution using mobile sensing system," in *Proceedings of International Solid State Sensors and Actuators Conference (Transducers' 97)*, vol. 1. IEEE, 1997, pp. 559–562.

[10] L. Marques, U. Nunes, and A. T. de Almeida, "Olfaction-based mobile robot navigation," *Thin solid films*, vol. 418, no. 1, pp. 51–58, 2002.

[11] A. J. Lilienthal, M. Reggente, M. Trincavelli, J. L. Blanco, and J. Gonzalez, "A statistical approach to gas distribution modelling with mobile robots-the kernel dm+ v algorithm," in *2009 IEEE/RSJ International Conference on Intelligent Robots and Systems*. IEEE, 2009, pp. 570–576.

[12] M. Reggente, "Statistical gas distribution modelling for mobile robot applications," Ph.D. dissertation, Örebro university, 2014.

[13] H. Ishida, G. Nakayama, T. Nakamoto, and T. Moriizumi, "Controlling a gas/odor plume-tracking robot based on transient responses of gas sensors," *IEEE Sensors Journal*, vol. 5, no. 3, pp. 537–545, 2005.

[14] A. J. Lilienthal, A. Loutfi, and T. Duckett, "Airborne chemical sensing with mobile robots," *Sensors*, vol. 6, no. 11, pp. 1616–1678, 2006.

[15] G. Ferri, E. Caselli, V. Mattoli, A. Mondini, B. Mazzolai, and P. Dario, "A biologically-inspired algorithm implemented on a new highly flexible multi-agent platform for gas source localization," in *The First IEEE/RAS-EMBS International Conference on Biomedical Robotics and Biomechatronics, 2006. BioRob 2006.* IEEE, 2006, pp. 573–578.

[16] W. Jatmiko, K. Sekiyama, and T. Fukuda, "A pso-based mobile robot for odor source localization in dynamic advection-diffusion with obstacles environment: theory, simulation and measurement," *IEEE Computational Intelligence Magazine*, vol. 2, no. 2, pp. 37–51, 2007.

[17] A. Gongora, J. Monroy, and J. Gonzalez-Jimenez, "Gas source localization strategies for teleoperated mobile robots. an experimental analysis," in *2017 European Conference on Mobile Robots (ECMR)*. IEEE, 2017, pp. 1–6.

[18] G. Reddy, V. N. Murthy, and M. Vergassola, "Olfactory sensing and navigation in turbulent environments," *Annual Review of Condensed Matter Physics*, vol. 13, no. 1, pp. 191–213, 2022.

[19] P. P. Neumann, V. Hernandez Bennetts, A. J. Lilienthal, M. Bartholmai, and J. H. Schiller, "Gas source localization with a micro-drone using bio-inspired and particle filter-based algorithms," *Advanced Robotics*, vol. 27, no. 9, pp. 725–738, 2013.

[20] Y. A. Prabowo, R. Ranasinghe, G. Dissanayake, B. Riyanto, and B. Yuliarto, "A bayesian approach for gas source localization in large indoor environments," in *2020 IEEE/RSJ International Conference on Intelligent Robots and Systems (IROS)*. IEEE, 2020, pp. 4432–4437.

[21] J. Ruddick, A. Marjovi, F. Rahbar, and A. Martinoli, "Design and performance evaluation of an infotaxis-based three-dimensional algorithm for odor source localization," in *2018 IEEE/RSJ International Conference on Intelligent Robots and Systems (IROS)*. IEEE, 2018, pp. 1413–1420.

[22] H. Zhu, Y. Wang, C. Du, Q. Zhang, and W. Wang, "A novel odor source localization system based on particle filtering and information entropy," *Robotics and autonomous systems*, vol. 132, p. 103619, 2020.

[23] X.-x. Chen and J. Huang, "Odor source localization algorithms on mobile robots: A review and future outlook," *Robotics and Autonomous Systems*, vol. 112, pp. 123–136, 2019.

[24] T. Jing, Q.-H. Meng, and H. Ishida, "Recent progress and trend of robot odor source localization," *IEEJ Transactions on Electrical and Electronic Engineering*, vol. 16, no. 7, pp. 938–953, 2021.

[25] M. Vergassola, E. Villermaux, and B. I. Shraiman, "'infotaxis' as a strategy for searching without gradients," *Nature*, vol. 445, no. 7126, pp. 406–409, 2007.

[26] T. Wiedemann, "Domain knowledge assisted robotic exploration and source localization," Ph.D. dissertation, Örebro University, 2020.

[27] L. Wang, S. Pang, and J. Li, "Olfactory-based navigation via model-based reinforcement learning and fuzzy inference methods," *IEEE Transactions on Fuzzy Systems*, vol. 29, no. 10, pp. 3014–3027, 2020.

[28] X. Chen, C. Fu, and J. Huang, "A deep q-network for robotic odor/gas source localization: Modeling, measurement and comparative study," *Measurement*, vol. 183, p. 109725, 2021.

[29] T. Wiedemann, C. Vlaicu, J. Josifovski, and A. Viseras, "Robotic information gathering with reinforcement learning assisted by domain knowledge: An application to gas source localization," *IEEE Access*, vol. 9, pp. 13 159–13 172, 2021.

[30] C. Bilgera, A. Yamamoto, M. Sawano, H. Matsukura, and H. Ishida, "Application of convolutional long short-term memory neural networks to signals collected from a sensor network for autonomous gas source localization in outdoor environments," *Sensors*, vol. 18, no. 12, p. 4484, 2018.

[31] O. Ronneberger, P. Fischer, and T. Brox, "U-net: Convolutional networks for biomedical image segmentation," in *Medical image computing and computer-assisted intervention–MICCAI 2015: 18th international conference, Munich, Germany, October 5-9, 2015, proceedings, part III 18*. Springer, 2015, pp. 234–241.

[32] K. He, G. Gkioxari, P. Dollár, and R. Girshick, "Mask r-cnn," in *Proceedings of the IEEE international conference on computer vision*, 2017, pp. 2961–2969.

[33] L.-C. Chen, G. Papandreou, I. Kokkinos, K. Murphy, and A. L. Yuille, "Deeplab: Semantic image segmentation with deep convolutional nets, atrous convolution, and fully connected crfs," *IEEE transactions on pattern analysis and machine intelligence*, vol. 40, no. 4, pp. 834–848, 2017.

[34] J.-G. Li, Q.-H. Meng, Y. Wang, and M. Zeng, "Odor source localization using a mobile robot in outdoor airflow environments with a particle filter algorithm," *Autonomous Robots*, vol. 30, pp. 281–292, 2011.

[35] A. N. Freedman, "The photoionization detector: Theory, performance and application as a low-level monitor of oil vapour," *Journal of Chromatography A*, vol. 190, no. 2, pp. 263–273, 1980.